Neuron
Article

Functional Properties of Cortical Feedback Projections to the Olfactory Bulb

Foivos Markopoulos,[1,2,3] Dan Rokni,[1,2] David H. Gire,[1] and Venkatesh N. Murthy[1,*]
[1]Molecular and Cellular Biology, and Center for Brain Science, Harvard University, Cambridge, MA 02138, USA
[2]These authors contributed equally to this work
[3]Present address: Department of Basic Neurosciences, University Medical Center, 1 Rue Michel-Servet, 1211 Genève 4, Switzerland
*Correspondence: vnmurthy@fas.harvard.edu
http://dx.doi.org/10.1016/j.neuron.2012.10.028

SUMMARY

Sensory perception is not a simple feed-forward process, and higher brain areas can actively modulate information processing in "lower" areas. We used optogenetic methods to examine how cortical feedback projections affect circuits in the first olfactory processing stage, the olfactory bulb. Selective activation of back projections from the anterior olfactory nucleus/cortex (AON) revealed functional glutamatergic synaptic connections on several types of bulbar interneurons. Unexpectedly, AON axons also directly depolarized mitral cells (MCs), enough to elicit spikes reliably in a time window of a few milliseconds. MCs received strong disynaptic inhibition, a third of which arises in the glomerular layer. Activating feedback axons in vivo suppressed spontaneous as well as odor-evoked activity of MCs, sometimes preceded by a temporally precise increase in firing probability. Our study indicates that cortical feedback can shape the activity of bulbar output neurons by enabling precisely timed spikes and enforcing broad inhibition to suppress background activity.

INTRODUCTION

The brain does not passively integrate sensory information to create a full and accurate representation of the sensory scene. Our everyday experience clearly shows that the brain can also suppress responses to stimuli that are of little importance, and attend to stimuli that are relevant or expected (Knudsen, 2007; Noudoost et al., 2010; Baluch and Itti, 2011). Most commonly, the behavioral state of an animal clearly modulates sensation and perception (Hurley et al., 2004; Fontanini and Katz, 2009). The underlying mechanism for these abilities is thought to involve the numerous connections through which information flows in a "backward" direction—from more central brain regions to peripheral ones (Knudsen, 2007; Restrepo et al., 2009; Noudoost et al., 2010; Baluch and Itti, 2011). Information about the importance of different stimuli can be used by the cortex to suppress or enhance responses in more peripheral structures.

The olfactory bulb (OB) receives input not only from the olfactory sensory neurons (OSNs), but also from the olfactory cortex and neuromodulatory inputs from other areas (de Olmos et al., 1978; Shipley and Adamek, 1984; Shepherd et al., 2004; Kiselycznyk et al., 2006; Matsutani and Yamamoto, 2008). Cortical inputs to the OB are diverse (Matsutani and Yamamoto, 2008), and are thought to mainly activate granule cells (GCs) (Price and Powell, 1970; Pinching and Powell, 1972; Davis et al., 1978; Davis and Macrides, 1981), which in turn inhibit mitral cells (MCs) and tufted cells (TCs) (Balu et al., 2007; Strowbridge, 2009). Some projections to the glomerular layer have also been described (Price and Powell, 1970; Pinching and Powell, 1972), but the exact targets there remain uncertain.

The functional properties of feedback connections have been described in a handful of studies in vitro using conventional stimulating electrodes (Balu et al., 2007; Nissant et al., 2009). It has been difficult to study the function of centrifugal inputs in vivo, in part because pharmacological methods are not feasible—cortico-bulbar synapses are glutamatergic, and therefore the use of pharmacological agents will affect peripheral inputs as well. In addition, feedback from different cortical areas such as the piriform cortex (PC) and anterior olfactory nucleus (AON; also called anterior olfactory cortex) may have different functional roles, but their axons cannot be easily isolated for electrical stimulation.

Here, we have used optogenetic methods to selectively activate feedback axons from the AON in vitro and in vivo, and examine their functional synaptic connectivity in the OB.

RESULTS

Virus Injections and Expression of ChR2 in AON Neurons

To stimulate the feedback connections from AON selectively, we expressed channelrhodopsin-2 (ChR2) in the AON of the right hemisphere of young rats (6–9 days old) by stereotactic injections of adeno-associated virus carrying the gene for ChR2 fused to the enhanced yellow fluorescent protein (EYFP) (Figure 1A) (Hagiwara et al., 2012). Expression of ChR2 was confirmed by examining EYFP fluorescence in the AON and the OB in brain slices, 2 weeks after injection. After adjusting the volume of injections, we were able to achieve consistent expression of ChR2 in neurons in the AON as well as in their axonal projections to the ipsilateral and contralateral OB (Figure 1B; see Figure S1

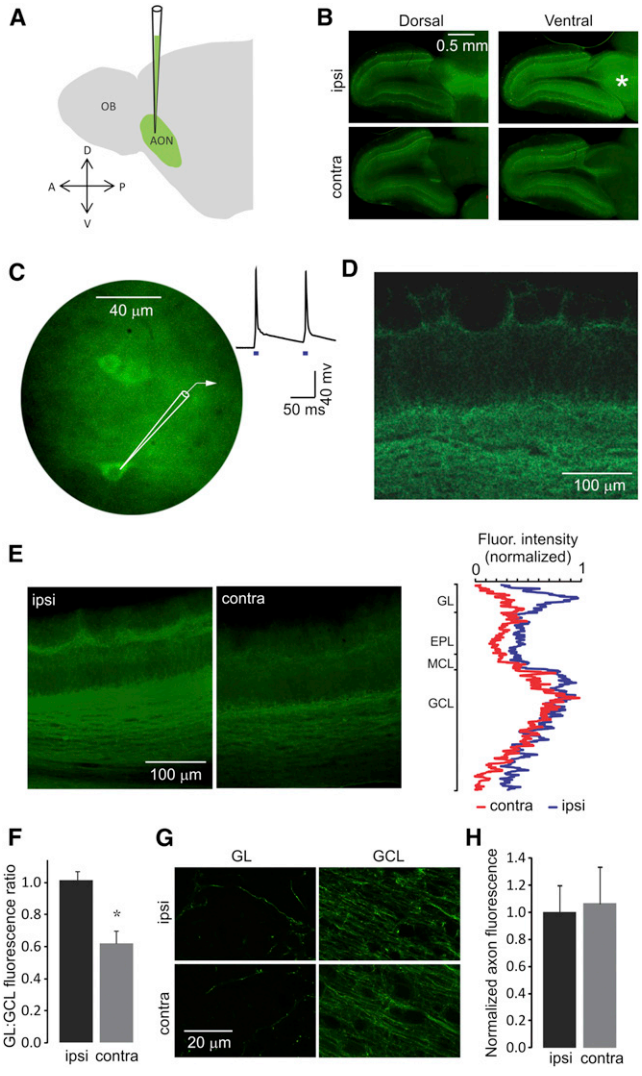

Figure 1. Virus Injections in the AON and ChR2 Expression in AON Axon Terminals in the OB

(A) Schematic representation of virus injections into the AON.

(B) Epifluorescence images showing expression of ChR2-EYFP in forebrain horizontal sections 2 weeks postinjection. ChR2-EYFP is expressed in the entire AON area of the right hemisphere (asterisk), as well as in its projections to the ipsilateral and contralateral OB.

(C) Blue-light stimulation evokes action potentials in AON neurons expressing ChR2-EYFP. Shown are AON neuron somata and a single trace recorded in the current-clamp mode. Blue squares in this and in the following figures denote light stimulation.

(D) Higher-magnification confocal image of the ipsilateral OB showing AON axons expressing ChR2-EYFP reaching all layers of the bulb.

(E) Epifluorescence images of the ipsilateral and contralateral OB. The fluorescence intensity profiles (right) show that AON axons reaching the glomerular layer are less prominent in the contralateral OB.

(F) The ratio between the fluorescence intensity of the glomerular and granule cell layers is significantly lower in the contralateral bulb (mean ± SD).

(G) High-magnification confocal images showing AON axons in the glomerular layer (GL) and the granule cell layer (GCL) of the ipsilateral and contralateral OB.

(H) Bar graph showing fluorescence intensity per single fiber in the ipsilateral and contralateral OB in the GL (mean ± SD). Values are not significantly different.

available online). Very few labeled cell bodies were detected in the OB (Figure S1), and even these are likely newborn GCs migrating from the rostral migratory stream—such cells take more than 3 weeks to release GABA (Bardy et al., 2010) and should not contribute significantly toward direct release upon light stimulation. To confirm functional expression of ChR2 in AON neurons, we obtained whole-cell patch-clamp recordings from AON neurons in acute slices from infected animals. Stimulation with blue light (whole field illumination, 5–10 mW/mm^2) depolarized AON neurons sufficiently to evoke action potentials (Figure 1C).

In fixed brain tissue, EYFP-positive axon terminals were clearly visible in the granule cell layer and the glomerular layer in both the ipsilateral and contralateral OB (Figure 1D). The fluorescence intensity of EYFP per area unit was not uniform across the different layers of the OB, with greater intensities in the granule cell layer and the bottom part of the glomerular layer; fluorescence intensities were distinctly lower in the external plexiform layer, where most of the dendrodendritic synapses between MCs/TCs and GCs are located (Figure 1E). Contralateral projections to the glomerular layer had lower intensity than those in ipsilateral glomerular layer, even when normalized to their corresponding granule cell layer intensities (1.02 ± 0.09 versus 0.62 ± 0.13, n = 3, $p < 0.05$; Figure 1F). These differences in average fluorescence intensities reflected the difference in density of fibers rather than expression levels of ChR2-EYFP, because the fluorescence intensity per area unit of single fibers in ipsilateral and contralateral OB were 1.00 ± 0.21 and 1.07 ± 0.28, respectively (n = 3 experiments, > 50 axons per experiment; errors are SD; Figures 1G and 1H), and not significantly different ($p > 0.1$).

Light Stimulation of AON Axon Terminals Evoked Synaptic Input to MCs In Vitro

We examined synaptic responses of MCs to AON stimulation using whole cell recordings in acute OB slices that were made 2 to 4 weeks postinjection (Figure 2A). Excitatory and inhibitory synaptic currents were recorded in the voltage-clamp mode at −70mV and 0mV, respectively, in response to a pair of 10 ms light pulses 100 ms apart. Although responses to pairs of stimuli are shown in the figures, all analysis reported below were done for the response to the first of the pair of stimuli. Light stimulation, unexpectedly, elicited excitatory as well as inhibitory synaptic currents in MCs, with inhibition being the dominant component (Figure 2B). All evoked currents were blocked by ionotropic glutamate receptor blockers (10 μM CNQX+ 100 μM APV; excitation blocked by 92.6% ± 4%, n = 3; inhibition blocked by 94.7% ± 3.1%, n = 4; $p < 0.01$; Figure 2C). Excitatory postsynaptic current (EPSC) amplitudes ranged from 5.8 to 29.1 pA and averaged 18.5 ± 6.6 pA (n = 15). The amplitude of EPSCs was not affected by gabazine (SR-95531, 10 μM; n = 4), which could largely abolish inhibitory postsynaptic currents (IPSCs) (Figure 2D). APV alone had no effect on EPSCs (n = 3, $p = 0.21$), and CNQX alone decreased EPSCs by 70.3% ± 30.3% (n = 3; $p < 0.01$). IPSCs, measured at 0mV, ranged from 19.2 to 1061.1 pA and averaged 316.3 ± 284.4 pA (n = 16). IPSCs were detected in 16 out of 16 cells (100%) recorded at 0mV, and EPSCs were detected in14 out of 15 cells (93.33%) recorded at −70mV.

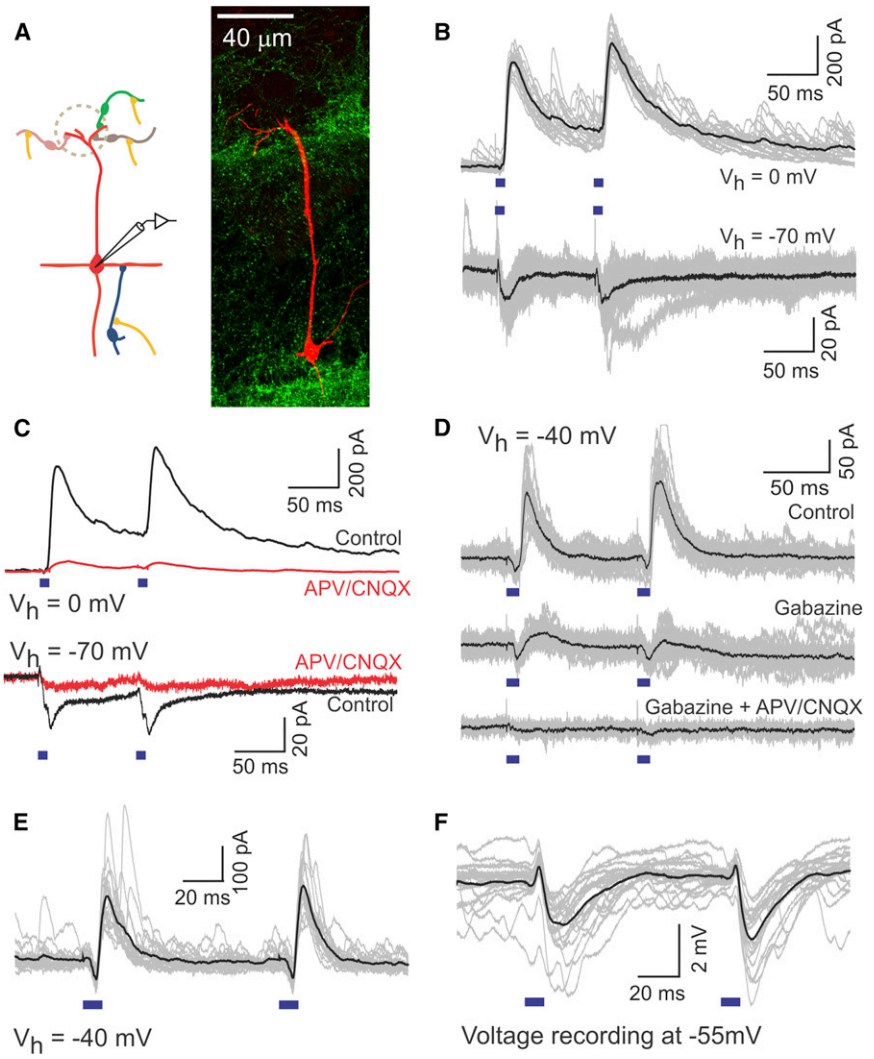

Figure 2. Light Stimulation of AON Axon Terminals in Slice Evokes Excitatory and Inhibitory Synaptic Currents in MCs

(A) A schematic illustrating the circuit (left) and a confocal image of a reconstructed MC filled with biocytin during recording (right).

(B) Light-evoked IPSCs (top) and EPSCs (bottom) recorded in different MCs at 0mV and −70mV, respectively. Black trace is the average of the individual traces shown in gray here and in the following figures.

(C) Both IPSCs (top) and EPSCs (bottom) are blocked by the application of glutamatergic blockers (APV 100 μM, CNQX 10 μM).

(D) Gabazine (10 μM) blocks light-evoked IPSCs without affecting EPSCs. Excitatory responses also disappear upon application of glutamatergic blockers.

(E and F) Light-evoked PSCs (E) and PSPs (F) recorded in a MC in voltage- (Vh = −40mV) and current-clamp (resting potential, Vm ~−55mV) modes, respectively. Both modes reveal both the excitatory and the inhibitory components. In MC recordings here and in other cell types below, synaptic responses to paired stimuli did not show a consistent trend for facilitation or depression.

When synaptic currents were recorded at −40mV, 11 out of 12 cells (91.67%) exhibited both IPSCs and EPSCs. IPSCs were delayed relative to EPSCs, with latencies of onset of EPSCs and IPSCs averaging 3.7 ± 0.8 ms (n = 15) and 10.5 ± 1.2 (n = 16), respectively (Figure S2). This delay difference indicates that inhibition from AON axons to MCs is disynaptic and excitation is most probably elicited by direct AON-to-MC synaptic connections. The relative timing and contribution of the two components was clearly evident when responses were recorded at a holding potential of −40mV (Figure 2E). As a consequence of the different delays, membrane potential recordings from MCs showed brief depolarization upon light stimulation, followed by hyperpolarization (Figure 2F). When recorded at resting potential (Vm ~−55mV), the average amplitudes of EPSPs and IPSPs were 0.57mV ± 0.25mV and 2.2mV ± 1.8mV, respectively (n = 13).

Sources of Light-Evoked Excitation in MCs

We investigated the source of the synaptic currents elicited by stimulation of AON axons, starting with excitation. We considered two possibilities: direct excitation of MCs and indirect excitation through excitatory local neurons.

Light-evoked excitation is blocked by ionotropic glutamate receptor blockers as described above (Figure 2) and shows an amplitude dependence with a reversal potential of 5.8mV ± 11.6mV (n = 4 cells). We next tested monosynaptic excitation directly using a previously described method (Petreanu et al., 2007; Gire et al., 2012; Hagiwara et al., 2012), in which transmitter release is evoked directly from ChR2-expressing axons in the presence of 1 μM tetrodotoxin (TTX) to remove polysynaptic excitation, 100 μM 4-AP to enhance axonal depolarization, and 10 μM gabazine. Four out of six recorded cells showed an excitatory current under these conditions, with an average amplitude of 10.5 ± 9 pA (range of 4.5–24 pA). Because the excitatory response persisted under these conditions, it is at least partly due to direct glutamate release from AON neurons without the involvement of intermediary neurons. We also tested if the response was due to extrasynaptic spillover of glutamate by using the weak competitive glutamate antagonist γ-DGG (Gire et al., 2012). Application of 500 μM γ-DGG, which is known to significantly attenuate spillover-mediated transmission between ETCs and MCs (Gire et al., 2012), did not significantly affect light-evoked EPSC amplitudes (percent block 0.2% ± 30%, n = 3 MCs). These features, as well as the short latencies of excitatory responses (Figure 2), suggest that at least part of the excitation arises from glutamate release from AON synaptic terminals directly on MCs.

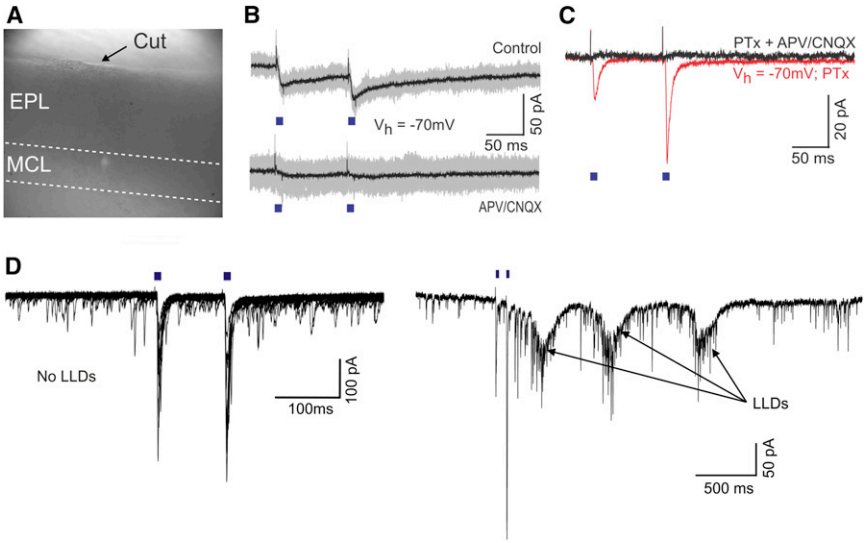

Figure 3. ETCs Receive Excitatory Inputs from AON but Are Not Required for Light-Evoked Excitation in MCs

(A) Widefield image showing a slice in which the glomerular layer was surgically removed.

(B) Light-evoked EPSCs recorded from a MC in a cut slice at −70mV. Responses are blocked by CNQX/APV.

(C) Light-evoked EPSCs recorded from an ETC in the presence of picrotoxin. Each trace is an average of 20 trials. Currents recorded before and after addition of CNQX/APV are shown in red and black, respectively.

(D) In a different experiment in the presence of gabazine, light stimulation occasionally evoked LLDs in an ETC. At left are 15 trials with no LLD, and at right is an example of a response with three LLDs (multiple LLDs only occur when inhibition is blocked). Note different time scales for the left and right traces. On average, LLDs occurred in 7.2% ± 9.3% of trials (n = 8 cells).

Because most of the known excitatory inputs to MCs target the tufts in the glomerular layer, we next asked whether AON excitatory inputs also target MC tufts. We recorded from MCs in slices where we had earlier performed a cut between the mitral cell layer (MCL) and the GL (Figure 3A). Light stimulation of AON axons in these cut slices evoked clear MC excitation, which could be abolished by APV/CNQX (n = 3; Figure 3B). The average amplitude of EPSCs in cut slices (16.6 ± 2.7 pA; n = 5) was similar ($p > 0.1$) to the amplitudes in regular slices (18.5 ± 6.6 pA; n = 15; Figure 2). Furthermore, the latency (3.8 ± 1.1 ms; n = 5) was also very similar ($p > 0.2$) to that found in uncut slices (3.7 ± 0.8 ms; n = 15). We also note that many MCs in uncut slices lacked the apical tuft, but nevertheless exhibited EPSCs.

Although the glomerular layer is not necessary for AON-triggered excitation in MCs, we wondered if additional excitation may arise through neurons in that layer. External tufted cells (ETCs) are plausible candidates because they are known to excite MCs (Hayar et al., 2004; De Saint Jan et al., 2009; Gire and Schoppa, 2009; Najac et al., 2011), and because AON axons project up to the glomerular layer (Figure 1). Therefore, we looked for monosynaptic EPSCs in ETCs, and for the so-called long-lasting depolarizations (LLDs) (Carlson et al., 2000), which signal glomerulus-wide activation (Gire et al., 2012). ETCs were identified based on their input resistance (50 MΩ ≤ Rm ≤ 200 MΩ) and the nature of their spontaneous synaptic inputs (Hayar et al., 2004) (Figure S3; see Experimental Procedures). In a few cases, they were also identified by their bursting activity in the cell-attached electrode configuration before whole cell access (Hayar et al., 2004). Stimulation of AON axons (in the presence of gabazine to isolate excitation) reliably evoked fast EPSCs in ETCs (Figure 3C), with an average amplitude of 58.5 ± 65.3 pA and an average latency of 3.8 ± 0.8 ms (n = 8). In addition, we also observed occasional LLDs in ETCs, which occurred in some of the trials (Figure 3D). On average, LLDs evoked by light stimulation were observed in only 7.2% ± 9.3% (n = 8) of trials, and occurred with latencies greater than 50 ms.

These results provide strong evidence that AON excites MCs directly and that these synapses are not located in the glomerular layer. Disynaptic excitation through ETCs is not a major component of AON driven excitation onto MCs.

Light-Evoked Inhibition in MCs Is Long Lasting and Partially Mediated by GCs

Activation of AON axons also evokes strong inhibition in MCs (Figure 2). Because this inhibition is abolished by glutamatergic blockers, the source of inhibition must be inhibitory interneurons within the bulb, which must receive excitatory inputs from the AON and synapse on MCs. We investigated possible synaptic inputs of the AON centrifugal axons to the main types of inhibitory interneurons in the OB. GCs, the most numerous inhibitory interneurons, are known to receive excitatory synapses from olfactory cortex feedback connections, and recent studies have shown that part of this excitation originates in the piriform cortex (Balu et al., 2007).

In voltage-clamp recordings from GCs, we observed light-evoked EPSCs that were sensitive to glutamatergic blockers (10 μM CNQX, 100 μM APV; block of 81.6% ± 21.2%, n = 4 cells, $p < 0.05$). We recorded mixed AMPA and N-methyl D-aspartate (NMDA) currents at +40mV and AMPA only currents at −70mV (Figure 4A). The latency of AMPA currents ranged from 2.5 to 5.7 ms with an average of 4.0 ± 1.1 ms (n = 7), indistinguishable from latencies of EPSCs to MCs. The amplitude of AMPA currents at −70mV ranged from 12 to 233 pA with an average of 79 ± 98 pA (n = 7). Current-clamp recordings confirmed that these inputs are sufficient to evoke action potentials in GCs, which occasionally outlasted the stimulus by 100 ms or more (Figure 4B). These results confirm that GCs receive glutamatergic inputs from the AON, acting on both AMPA and NMDA receptors.

Inhibition in MCs evoked by stimulation of the sensory nerve, or MCs themselves, lasts for hundreds of milliseconds due to asynchronous release of GABA from GCs onto MC dendrites (Isaacson and Strowbridge, 1998; Schoppa et al., 1998; Kapoor and Urban, 2006). We examined whether inhibition evoked by AON stimulation has a similar time course. We obtained voltage-clamp recordings from MCs at 0mV, using a single pulse

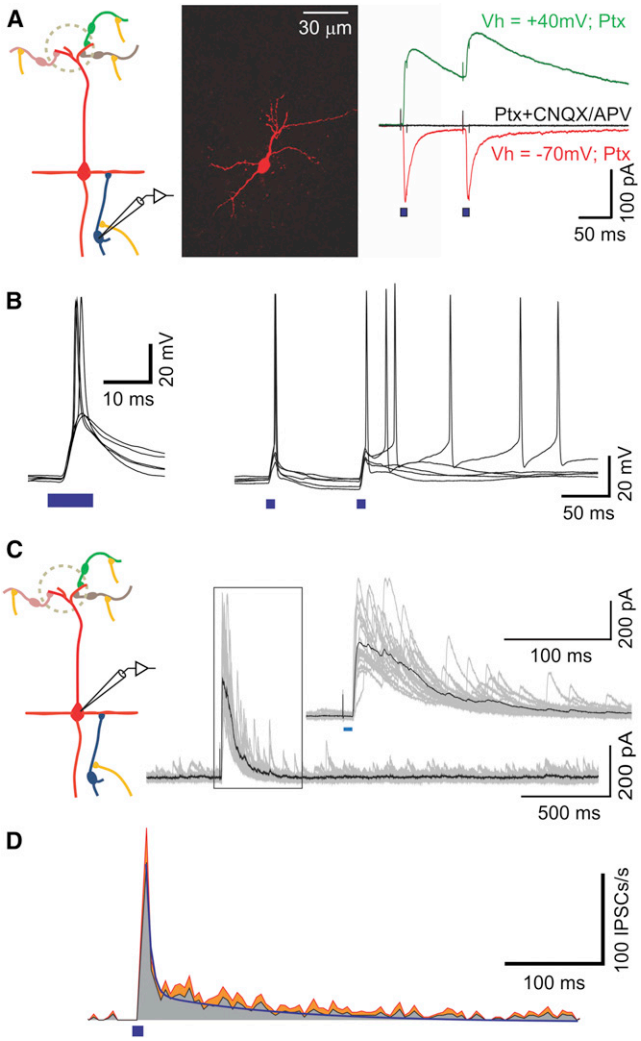

Figure 4. Light-Evoked Inhibition in MCs Is Partially Mediated by GCs

(A) Illustration of the circuit (left), a confocal image of a reconstructed GC filled with biocytin during recording (middle) and light-evoked EPSCs recorded from a GC in the presence of picrotoxin (right). Each trace is an average of 20 trials. Mixed AMPA and NMDA currents recorded at +40mV are shown in green, AMPA only currents recorded at −70mV are shown in red and recording with CNQX/APV at +40mV is shown in black.

(B) Light-evoked action potentials in a GC.

(C) Light-evoked IPSCs recorded from a MC at 0mV with single-pulse stimulation, showing long-lasting inhibitory responses. The insert shows a magnification of the framed area.

(D) Average PSTH of the single-pulse light-evoked IPSCs from six MCs. The SEM is shown in red. The biexponential fit is shown as a continuous blue line.

of light (10 ms). Light stimulation evoked a barrage of IPSCs, lasting for hundreds of milliseconds (Figures 4C and 4D). We detected individual events and obtained a histogram of all events from multiple recordings (Figure 4D). Spontaneous IPSCs occurred at an average rate of 1.6 ± 0.5 events/s (n = 6), and increased to 173.3 ± 93.5 events/s immediately after light stimulation. The decay of these events to baseline occurred with a time course that could be fitted with two exponentials with time constants of 6.4 ± 10.3 ms and 135 ± 47 ms, with the slower component accounting for more than 80% of the events.

These results suggest that AON-derived inputs to GCs can depolarize these cells and evoke action potentials, thereby driving GABA release from GCs onto MCs dendrites.

Feedback Inhibition in MCs Also Arises in the Glomerular Layer

In addition to inhibition from GCs, MCs also receive inhibitory synapses in the glomerular layer (Shao et al., 2012). To reveal other potential sources of light-evoked inhibition in MCs, we obtained voltage-clamp recordings from juxtaglomerular cells. All cell types we recorded from displayed excitatory responses to AON stimulation (Figure 5). We identified GABAergic juxtaglomerular cells following established electrophysiological criteria (Hayar et al., 2004) (Figure S3), which are described in the Experimental Procedures. Both periglomerular cells (PGCs) and short axon cells (SACs) responded to light stimulation with EPSCs that had both AMPA and NMDA components (Figures 5A and 5B). In PGCs, AMPA currents had a latency ranging from 2.5 to 6.9 ms, with an average of 4.2 ± 1.3 ms (n = 10). The amplitude ranged from 5.00 to 167 pA and had an average of 44 ± 47 pA (n = 10). In suspected SACs, AMPA currents had a latency ranging from 2.5 to 5.0 ms, with an average of 3.5 ± 1.1 ms (n = 8). The amplitude ranged from 8 to 154 pA and had an average of 53 ± 57 pA (n = 8). Our data provide functional evidence that glomerular layer GABAergic cells receive excitatory inputs from the AON, and therefore are in a position to inhibit MCs.

To estimate the contribution of the glomerular layer to the AON-evoked inhibition of MCs, we obtained recordings from MCs before and after blocking inhibition in the GL with local application of the $GABA_A$ receptor blocker gabazine (SR-95531, 100 μM). In patched MCs, filled with biocytin-Alexa 594, we were able to visualize the apical dendrite and apply gabazine locally over the apical dendritic tuft (Figure 5C). This led to a reversible reduction of light-evoked IPSCs by 32% ± 3.5% (Figure 5D; n = 3, $p < 0.05$). To verify the specificity of gabazine application, we also applied gabazine in a neighboring glomerulus, which had a negligible effect on light-evoked IPSCs amplitude (a reduction of only 8.7%; data not shown). We performed additional control experiments to confirm the efficacy of locally applied gabazine in blocking $GABA_A$ receptors in the glomerulus and to confirm that gabazine did not significantly affect granule to mitral cell inhibition (Figure S4).

These results indicate that part of the disynaptic inhibition in MCs triggered by AON activity arises in the glomerular layer.

Light Stimulation of AON Axon Terminals Modulates MCs Firing In Vitro

To understand the functional significance of the combined excitatory and inhibitory input from the AON onto MCs, we next tested how this input might affect suprathreshold activity of MCs. For these experiments, we switched to a potassium-based internal solution and recorded MC responses to light stimulation of AON inputs in the current-clamp mode.

MC responses to light stimulation were recorded at three different membrane potentials: (1) resting membrane potential,

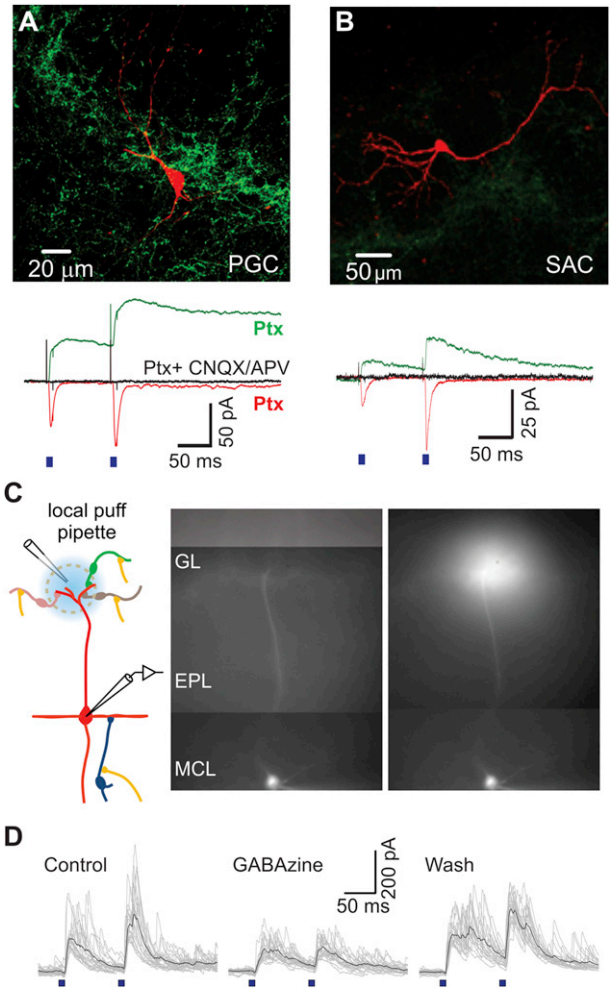

Figure 5. Light-Evoked Inhibition in MCs Is Also Mediated by Glomerular Layer Interneurons

(A and B) Top: confocal images of a reconstructed PGC (A) and SAC (B) filled with biocytin during recordings. Bottom: light-evoked EPSCs recorded from the PGC (A) and the SAC (B) in the presence of picrotoxin. Each trace is an average of 20 trials. Mixed AMPA and NMDA currents recorded at +40mV are shown in green, AMPA-only currents recorded at −70mV are shown in red, and block with CNQX/APV at +40mV is shown in black.

(C) Left: experimental setup for focal block of inhibition in the glomerular layer during recordings from MCs. Right: epifluorescence images of a MC filled with biocytin-Alexa 594 before and while recording and puffing of gabazine on its apical dendrite's tuft. The puff solution also contained Alexa 594.

(D) Light-evoked IPSCs in MCs before (left), during (middle), and after (right) local application of gabazine in the glomerular layer. The reduction of IPSCs by 30% reflects the weight of juxtaglomerular cells' contribution to the light-evoked inhibition observed in MCs.

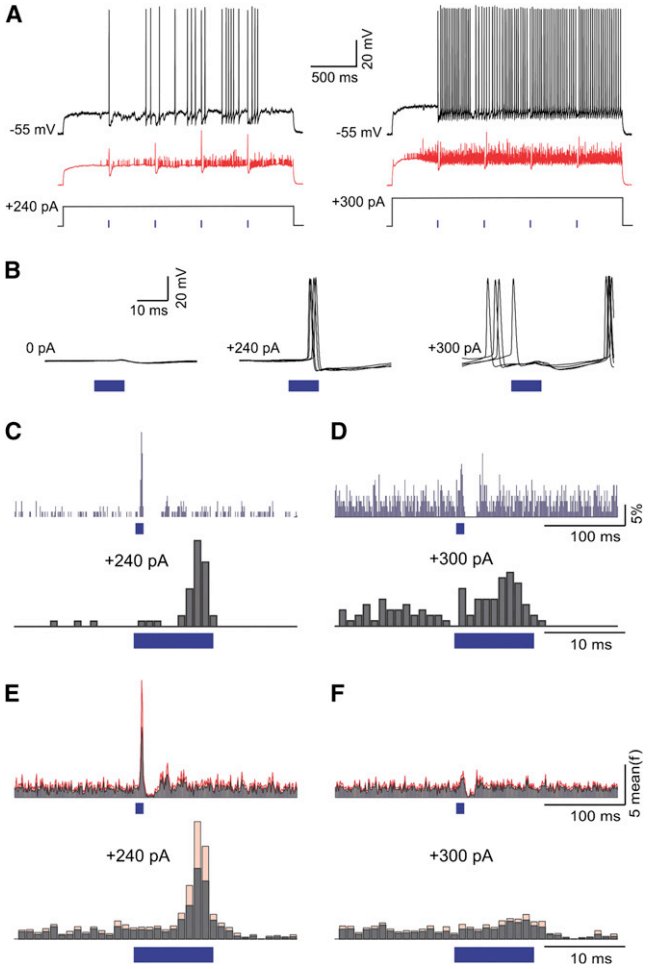

Figure 6. AON Inputs' Effect on MC Firing Is Dependent on Basal Activity Levels

(A) The responses of a MC to AON inputs when either moderately (left) or highly (right) active. Moderate and high activity levels were achieved by injection of 240 and 300 pA, respectively. Black trace is a single trial and red trace is the average of 20 trials.

(B) Five superimposed traces of the mitral cell's response to AON stimulation at resting membrane potential (left), with 240 pA current injection (middle), and with 300 pA current injection (right). Note that AON stimulation induced precisely timed spikes with 240 pA current injection, but induced a pause in spiking with injection of 300 pA.

(C and D) PSTHs of spike probability with 240 (C) and 300 (D) pA current injection for an exemplar cell with light stimulation at lower (top) and higher (bottom) magnification. Time bins are 1 ms.

(E and F) Normalized population PSTHs of spike probability at different depolarization steps (n = 6 cells) with light stimulation at lower (top) and higher (bottom) magnification. Gray lines show the mean and red lines show SEM. Time bins are 1 ms.

where typically MCs are quiescent in slice preparations; (2) just above threshold, where MCs tend to fire irregularly at low rate; and (3) well above threshold, where MCs fire more regularly at high rates (Figure 6). Activating AON inputs when a MC was at resting potential did not induce spiking, indicating that the direct excitation from AON neurons onto MCs may be too weak to activate them (Figure 6B, left traces). When the cell was near threshold, AON stimulation was able to elicit action potentials reliably as shown in five sample trials (Figure 6B, middle). When well above firing threshold, activation of AON input elicited pauses in firing that were followed by rebound firing (Figure 6B, right).

We quantified the effects of AON stimulation by generating peristimulus time histograms (PSTHs, 1 ms bins) at the two different levels of baseline activity in MCs (Figures 6C–6F). Example PSTHs from one cell are shown in Figures 6C and 6D. When the MC was in the low firing rate regime, a clear increase in firing could be observed during light stimulation, followed by a decrease (Figure 6C). When the same MC was firing at a higher rate, excitation was less prominent (Figure 6D). We analyzed the significance of the excitatory effect by comparing our data to 100,000 randomly aligned histograms (see Experimental Procedures for details). We found three of six cells to have a significant excitatory response ($p < 0.01$).

Population analysis of these experiments, with the firing rate of each cell normalized to the prestimulus period, is shown in Figures 6E and 6F. With 240 pA current injection, AON input had a dual effect consisting of a brief increase in firing probability followed by a more prolonged decrease. On average firing probability was increased to a peak of 9.5 ± 11.3 times the baseline with a latency of 7 ± 1.7 ms ($n = 6$; Figure 6E). The average firing in the 10 ms periods of light stimulation was 5 ± 7.8 times the rate during the 10 ms right before stimulation ($n = 6$, $p < 0.01$, rank-sum test). In the 15 ms following light stimulation, firing was reduced to 0.4 ± 0.5 of baseline values ($p < 0.05$, rank-sum test) (Figure 6E). With 300 pA, AON input had a smaller effect on firing probability during light stimulation, increasing it to a peak of 2.0 ± 0.5 times the baseline, and an average increase of 1.8 ± 0.7 times baseline values in the 10 ms period of light stimulation ($n = 6$; $p < 0.01$, rank-sum test). The inhibitory effect with 300 pA was manifested as a decrease of the average firing rate to 0.5 ± 0.5 of baseline values ($p < 0.05$, rank-sum test; Figure 6F). This inhibition was followed by a rebound increase in firing rate presumably due to the intrinsic biophysical properties of MCs (Balu and Strowbridge, 2007).

These results indicate that AON inputs can have multiple effects on MCs, depending on their ongoing activity, in part due to the newly discovered direct excitatory inputs.

Light Stimulation of AON Axon Terminals Inhibits MC Firing In Vivo

We next tested the functional significance of the AON inputs to MCs in vivo. We used tungsten electrodes to record the activity of single MCs from the dorsal OB in anesthetized rats 2–4 weeks postinjection of the virus. Breathing was continuously monitored with a piezoelectric belt that was wrapped around the rat's torso and a light stimulus consisting of a pair of 40 ms stimuli, separated by 50 ms, was delivered every 15 s.

Putative MCs/TCs were identified based on their depth and their strong breathing related firing pattern (Macrides and Chorover, 1972). Previous studies have noted that GCs are not visible to extracellular electrodes (Kay and Laurent, 1999; Rinberg et al., 2006; Doucette et al., 2011). Figure 7A shows an example of such an experiment. Single units were identified by stereotyped spike waveforms identified using cluster analysis (Figure 7A1). Figure 7A2 shows five traces aligned by the light stimulus (blue square). Because MC firing patterns consist of short breathing-related bursts and pauses, it was not easy to see the effect of AON stimulation within a few trials. However, when pooling more trials, one can easily see the inhibitory effect of the stimulus as a consistent gap in firing that outlasts the stimulus by roughly 100 ms (Figure 7B). For the analysis of the inhibitory effect, we constructed PSTHs using 20 ms time bins. This example cell had an average spontaneous firing rate of 11.9 spikes/s, which decreased by 93% to 0.8 spikes/s upon stimulation of AON axons (Figure 7C). Across experiments, light stimulation of AON axons led to a reduction of firing by 58% ± 31% ($p < 0.01$), which recovered with a time constant of 189 ms ($n = 20$; Figure 7D top). No such effect was observed in noninjected control animals ($n = 12$; Figure 7D bottom).

We also tested the effects of AON activation on odor-evoked responses in MCs. We used a custom-built olfactometer to deliver up to three different odors to anesthetized rats with ChR2 expression in AON. Light stimuli were delivered 3.5 s after onset of odor stimulus (Figure 7E). In units that showed increased firing rate upon odor stimulation, brief light pulses rapidly suppressed firing, which recovered upon termination of light stimuli (Figure 7E). On average, AON stimulation suppressed odor-evoked responses by 66% ± 33% ($n = 9$ cells from five animals; $p < 0.01$ compared to prestimulus firing rate; Figure 7F). The degree of suppression was not different from that observed for spontaneous firing ($p > 0.5$).

Because MCs have a tendency to fire at specific phases of the breathing cycle (Figure 7G) (Macrides and Chorover, 1972), we asked whether the effect of AON activation will depend on the phase in which it arrives in the breathing cycle. For this analysis, we split the data from the experiments on spontaneous MC activity into two separate histograms: one for all stimuli that arrived at the preferred half of the cycle (where MCs tend to fire, Figure 7H) and one for the stimuli that arrived at the nonpreferred half of the cycle (Figure 7I). Because the baseline for these histograms is not flat (reflecting the breathing dependent modulation of MC activity), it is harder to visualize the effect of stimulation. We therefore generated control histograms that are aligned by a "sham" stimulus at 1Hz (Figures 7H and 7I, middle panels). The subtraction of these sham histograms from the AON stimulus aligned histograms shows the net effect on firing rate (Figures 7H and 7I, bottom panels). AON stimulation was able to inhibit MC firing in both halves of the breathing cycle in the population data (Figures 7J and 7K). The integrated effect over 500 ms was significant in both conditions. Light stimulation reduced firing by 36% ± 27% ($p < 0.01$, $n = 9$) when it coincided with the high firing phase, and by 39% ± 30% ($p < 0.01$, $n = 9$) when it coincided with the low firing phase. Although the inhibition seemed more transient for "in-phase" stimulation, the integrated effect over 500 ms was not significantly different between the two conditions ($p > 0.5$, $n = 9$) probably due to the prolonged inhibitory effect of AON stimulation.

Activation of AON Axon Terminals Can Trigger Precise Spiking in MCs In Vivo

Using 50 ms bins, we were unable to find evidence for fast excitation that was observed in the in vitro experiments. We therefore constructed PSTHs using 1 ms bins. By comparing these PSTHs to randomly aligned PSTHs, we found significant fast excitation in 9 out of 20 cells (see Experimental Procedures). An example of this excitation is shown in Figure 8. While only inhibition was seen

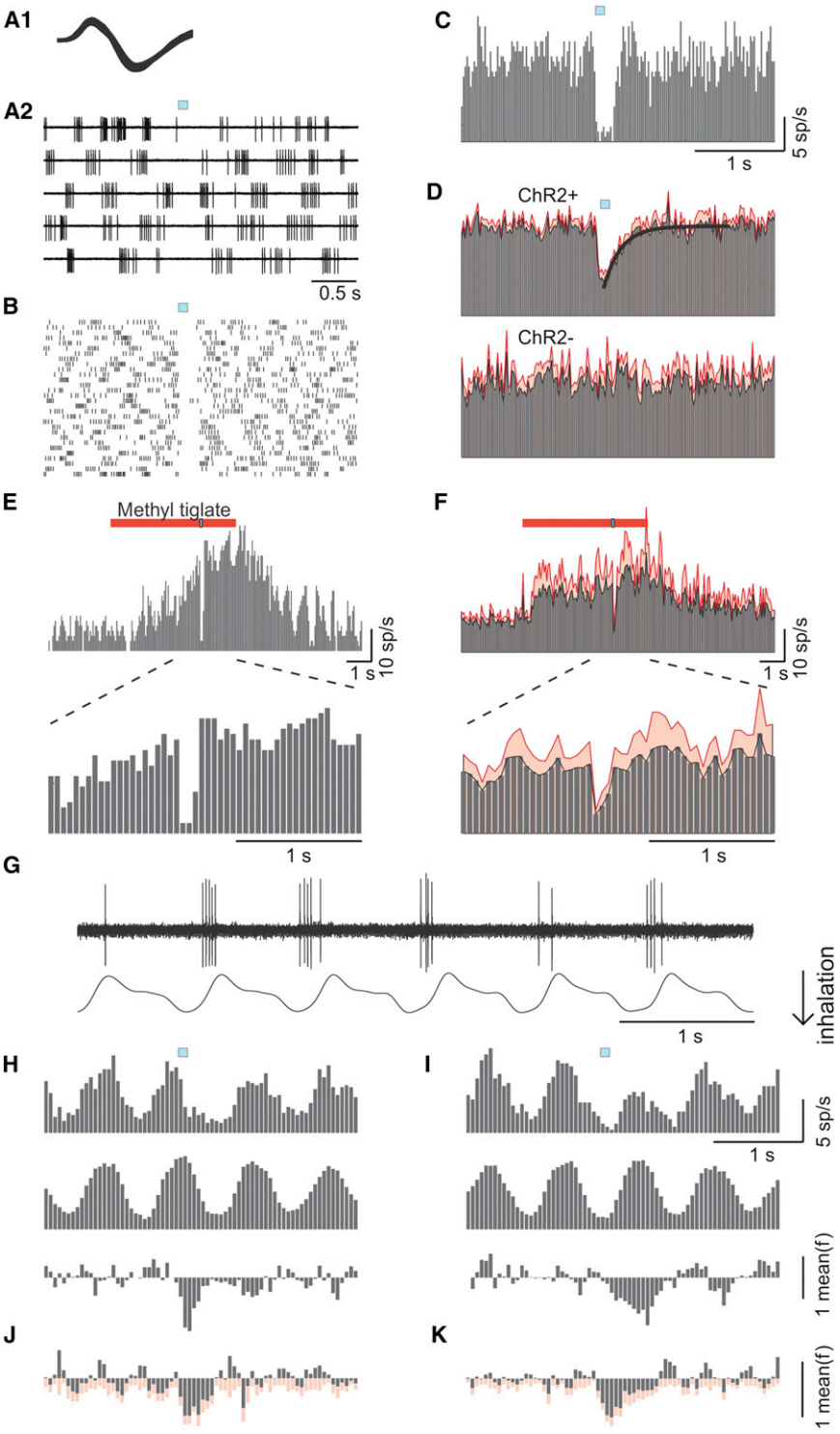

Figure 7. Light Stimulation of AON Axon Terminals In Vivo Reduces Spontaneous and Odor-Evoked Firing in MCs Independently of Breathing Timing

(A–C) The response of an exemplar cell to light activation of AON fibers. (A1) Superimposed spikes recorded from the cell. (A2) Raw traces aligned to light stimulation (blue square) showing the firing of that cell. (B) Raster plot of the cell's action potentials in 30 trials of light stimulation. (C) PSTH constructed from 60 trials of light stimulation. Time bins are 20 ms.

(D) Population PSTHs of cells recorded from ChR2-expressing animals (ChR2+, n = 20 cells) and from control animals (ChR2−, n = 12 cells). The mean is shown in gray and the SEM in red. The continuous line in the top PSTH is a best-fitting single exponential function.

(E) PSTH of spikes from an exemplar cell responding to the odor methyl tiglate (red bar, 5 s presentation), and being inhibited by light stimulation at 3.5 s after odor onset (blue square embedded in the red). The PSTH expanded around the light stimulation clearly illustrates inhibition of spikes.

(F) Population PSTH of all cells (n = 9 cells) responding to multiple odors, with SE shown in red. Time bins for odor-evoked PSTHs are 50 ms.

(G) A simultaneous recording of MC activity and the animal's respiration. Note that action potentials tend to occur in the time of the transition from inhalation to exhalation.

(H and I) The effect of AON input during the preferred (H) and nonpreferred (I) half of the breathing cycle, for an exemplar cell. Top panels show PSTHs for light stimuli arriving at the preferred (H) and nonpreferred (I) half of the breathing cycle. Middle panels show sham PSTHs that are generated by a 1 Hz sham signal for comparison purposes. Bottom panels show the effect of the AON input as measured by subtracting the sham PSTHs from the light-evoked PSTHs. Units of firing rates are normalized to the mean firing rate.

(J and K) Population analysis (n = 9 cells) of the effect of AON input on the preferred (J) and nonpreferred (K) half of the breathing cycle. Mean is shown in gray and SEM in red. Time bins for (H–K) are 50 ms.

with 50 ms bins (Figure 8A), a very brief and precise excitation was evident with finer binning (Figure 8B). Excitation in this cell was manifested as a 1 bin (1 ms) of increased probability of firing from 1% to 8.9%, with a latency of 5 ms (Figure 8C). This latency was markedly different from the latency to the photoelectric artifact that always coincided with the first bin of light stimulation (Figure 8D). On average, AON axon stimulation increased firing probability 9.5 ± 3.3 times with a latency of 6 ± 1.8 ms (n = 9). Average population PSTHs pooling data from the nine cells that were excited by the AON fibers and of the whole population, are shown in Figure 8E. Figure 8F shows the nine cell histogram at an enlarged scale. The duration of the excitatory response in the average PSTH mostly reflects the variability in the latency among the cells. Indeed, if responses were aligned on the peaks of each cell's excitation, the average PSTH exhibited a narrow peak of less than 5 ms (Figure 8G).

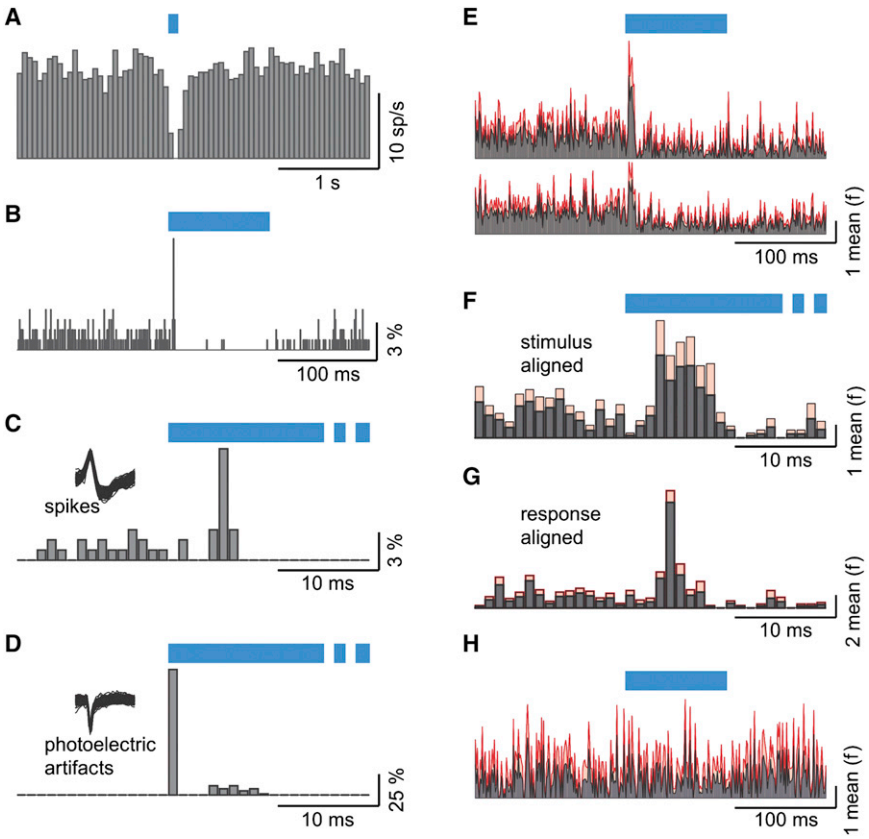

Figure 8. Excitation of MCs by AON Axons Is Manifested as Accurately Timed Spikes In Vivo

(A–D) Data recorded from one cell. (A) A PSTH using time bins of 50 ms. (B) A PSTH of the same data as in (A) but with 1 ms time bins. The height of the bars indicates the percentage of trials in which firing occurred within the corresponding time bin. (C) The same PSTH as in (B), shown in an enlarged scale. (D) PSTH as in (C) but for the optoelectric artifact that is produced by shining light on the metal electrode. Note the difference in latency between the biological action potentials and the artifact.

(E–G) Population PSTHs from cells in which excitation was statistically identified. Mean is shown in black and SE in red. Firing probabilities are normalized to the mean (E). Population PSTH obtained with 1 ms bins. Top PSTH is for 9 of 20 cells in which a statistical test identified excitation. Bottom PSTH is for all 20 cells. (F) The same PSTH as in E (top), shown in an enlarged scale. (G) A peristimulus time histogram. The histogram is aligned to the response peak and not to the stimulus. Note the difference between (F) and (G) indicating that the breadth of the PSTH in (F) is mostly due to the latency differences between different experiments and not to the jitter of any one cell. (H) Population PSTH at 1 ms bin resolution for 11 cells from control animals.

Importantly, no excitation was evident in any of the control cells (n = 11, Figure 8H). We did not find any evidence of rapid excitation in odor-evoked responses.

These results reveal that activation of AON axons in vivo leads to an immediate and brief increase in firing probability of MCs, followed by a longer lasting inhibition.

DISCUSSION

We used optogenetic methods to selectively activate feedback axons to the OB, and determine their cellular targets and their functional effects on bulbar output neurons. The major findings of our study are that: (1) AON axons have a dual effect on MCs: fast, brief depolarization and more prolonged hyperpolarization, (2) the fast depolarization is likely to be due to direct monosynaptic excitation, (3) the inhibitory effect of AON activation on MCs is mediated through GCs as well as glomerular layer interneurons, and (4) as a result of these synaptic effects, activation of AON axons could impose precisely timed spikes on output neurons, followed by suppression of spikes for tens of milliseconds. Broadly similar results, but with some interesting specific differences, have been reported for feedback projections from the piriform cortex in independent work (Boyd et al., 2012).

Selective Activation of AON Feedback

Cortical inputs to the OB are diverse (Price and Powell, 1970; Pinching and Powell, 1972; Davis et al., 1978; Davis and Macrides, 1981) and have generally been thought to mainly activate GCs in the OB, which in turn inhibit MCs and TCs (Balu et al., 2007). Although some projections to the glomerular layer have also been described anatomically, their origins and cellular targets there have remained uncertain (Davis and Macrides, 1981; Matsutani and Yamamoto, 2008). The functional properties of feedback connections have been described in a handful of studies in vitro using conventional stimulating electrodes (Balu et al., 2007; Nissant et al., 2009), which lack specificity because axons from many sources (for example, AON and PC) mingle freely not only among themselves, but also with feedforward projections (Powell et al., 1965; Price and Powell, 1970). The two major cortical sources of feedback—the AON and PC—are likely to have different functional roles (Brunjes et al., 2005; Lei et al., 2006; Rennaker et al., 2007; Kikuta et al., 2008, 2010; Stettler and Axel, 2009; Isaacson, 2010), and their projection pattern to the OB may also have significant differences (Davis and Macrides, 1981). Therefore, studying these two sources of feedback separately is essential to dissect their specific roles, and optogenetic tools allow selective activation (Miesenböck, 2009; Deisseroth, 2011). Here, we targeted viral expression of ChR2 in AON using stereotactic surgeries. Although the AON has subdivisions, which may have distinct projection patterns (Reyher et al., 1988; Brunjes et al., 2005; Illig and Eudy, 2009), we have chosen to treat the AON as a single entity here. Future studies can examine more closely the contributions of the different subregions of the AON.

Robust AON Projections to the Glomerular and GC Layers

Classic anatomic studies have uncovered robust cortical projections to deeper layers of the OB, where they are thought to make synapses on GCs (Price and Powell, 1970; Pinching and Powell, 1972; Davis et al., 1978; Davis and Macrides, 1981). Some projections to the glomerular layer have also been described (Price and Powell, 1970; Pinching and Powell, 1972; Davis et al., 1978; Davis and Macrides, 1981), but the exact targets have remained uncertain. We found that axons from the AON project to the granule cell and glomerular layers. Interestingly, superficial axons appear to be concentrated at the edges of glomeruli, with little penetration into the interior. This suggests that synapses are made on the somata or proximal dendrites of glomerular neurons rather than in the dendrites within the glomeruli.

We found that AON axons also project to the contralateral OB as noted previously (Davis and Macrides, 1981), but these projections were relatively sparse in the glomerular layer. Because glomerular layer interneurons can have a significant role in mediating disynaptic inhibition on MC, ipsilateral and contralateral AON projections may affect MCs in distinct ways. The weaker contralateral projections were not due to lower levels of ChR2, because fluorescence intensity of individual axons and boutons was similar to ipsilateral projections. The contralateral projections were functional because disynaptic inhibition could be evoked in MCs, although the total amount of inhibition was lesser than matched measurements from ipsilateral MCs (Figure S5). There is evidence for preferential ipsilateral versus contralateral projections from different subregions of the AON (Reyher et al., 1988; Brunjes et al., 2005), and future studies targeting ChR2 expression to specific subregions may reveal functional specializations.

MCs Receive Direct Excitation from AON

Based on previous studies, we expected to see disynaptic inhibition in MCs when AON axons were stimulated. Unexpectedly, we found that MCs receive not only inhibition but also direct excitation. A synaptic origin of this excitation is supported by the following observations: (1) the reversal potential of EPSCs was close to 0mV, as expected for ionotropic glutamatergic currents; (2) light-evoked currents are blocked by ionotropic glutamatergic receptor blockers; and (3) the currents persist when polysynaptic activity is minimized with TTX. Additional experiments also offer strong support for direct excitation from the AON. First, the latency of these events was the same as the latency of EPSCs in all other cells examined in our study (Figure S2). Second, EPSCs persisted even in the absence of MC primary tufts in the glomerular layer, or even in the complete absence of the glomerular layer itself—ruling out a sole contribution from ETCs, which are the only identified local source of excitation for MCs.

Our experiments with the low-affinity γ-DGG also indicate that the excitation is due to synapses made directly on MCs, and not through extrasynaptic activation of MC glutamate receptors, which mediates dendrodendritic self-excitation (Nicoll and Jahr, 1982; Christie and Westbrook, 2006; Pimentel and Margrie, 2008). Because the glomerular layer is dispensable for this excitation of MCs by AON, and there is negligible innervation of AON axons in the EPL where MC lateral dendrites are, the likely locus of MC excitation is the cell body layer. Independent of the exact mechanism of depolarization, AON axons are able to evoke time-locked spikes in MCs at least under some conditions. The direct excitation followed by disynaptic inhibition establishes a small time window within which MCs can emit spikes, reminiscent of the action of many feedforward circuits throughout the brain (Pouille and Scanziani, 2001; Isaacson and Scanziani, 2011).

Disynaptic Inhibition Is Powerful and Long Lasting

Robust inhibition is evoked in MCs following activation of AON axons, leading to a pause in firing for tens of milliseconds. The latency of inhibition, as well as its indirect blockade through glutamatergic receptor antagonists, confirms its disynaptic origin. At least part of the inhibition arises through GCs, which receive monosynaptic excitation from AON. GC-mediated inhibition has most often been studied using sensory inputs in the OB, either by directly stimulating OSNs or by stimulating MCs (Isaacson and Strowbridge, 1998; Schoppa et al., 1998; Egger and Urban, 2006). Recently, it was shown that activating putative feedback axons can cooperatively enhance dendrodendritic inhibition evoked by MC stimulation (Balu et al., 2007). We found that inhibition in MCs has a robust fast component, followed by delayed synaptic events that last longer than 100 ms. The fast component of inhibition accounted for only about 20% of the total charge, but because of its synchronous nature can lead to strong suppression of activity.

It has been known for some time that elementary inhibitory events from GCs evoked by MC activation continue to occur for hundreds of milliseconds (Isaacson and Strowbridge, 1998; Schoppa et al., 1998). Here, we find that similar delayed events can occur after activation of GCs through AON axons, but the time constant of these events is shorter than that reported for dendrodendritic inhibition evoked by depolarizing MCs (Isaacson and Strowbridge, 1998; Schoppa et al., 1998). This difference could be due to the manner in which GCs are activated: cortical axons appear to target proximal dendrites of GCs and evoke larger quantal events with faster kinetics, whereas MC synapses are made on distal dendrites, have lower amplitudes and slower kinetics. These differences could lead to more gradual depolarization of GCs when MCs are active, allowing the A-type potassium currents to delay spiking in GCs. We found that activation of AON synapses often results in immediate spiking of GCs within a few milliseconds, perhaps due to the larger amplitude, faster synaptic inputs.

Rapid inhibition in MCs triggered by activation of AON axons appears to be well-placed to impose timing constraints on MC spiking. Because MC spike timing has clearly been shown to be an important part of odor information leaving the OB (Cury and Uchida, 2010; Dhawale et al., 2010; Shusterman et al., 2011), the AON is in a key position to influence it.

Routing of Feedback Inhibition through Glomerular Layer

Although anatomical studies have identified glomerular innervation of AON axons, no functional studies have been undertaken until now due to the difficulty in selectively stimulating AON axons. Here, by optical stimulation of identified AON axons, we

have identified several target neurons in the glomerular layer including ETCs, PGCs, and SACs. Although AON axons excited ETCs, they rarely evoked LLDs, which lead to glomerulus-wide excitation and large depolarizations in MCs (Gire et al., 2012). The direct excitation of glomerular interneurons by AON, combined with the absence of glomerular LLDs, results in a net inhibition to MCs. In fact, our experiments suggest that more than 30% of the transient inhibition on MCs arises from the glomerular layer. Remarkably, cortical feedback is capable of influencing information flow at the very first synaptic processing stage in the OB. Glomerular inhibition can be effective in shunting out sensory input because MCs may rely on input from ET cells more than direct sensory nerve input (Najac et al., 2011; Gire et al., 2012). Therefore, cortical feedback to the glomerular layer may have differential effects on odor-evoked responses of TC and MCs—for example, inhibiting TCs less than MCs. Finally, AON activation of glomerular interneurons could also lead to presynaptic inhibition of sensory nerve terminals (Pírez and Wachowiak, 2008; Petzold et al., 2009).

It is not clear whether feedback routed through the glomerular layer is a unique feature of the AON. Backprojections from PC may not extend to the glomerular layer, in contrast to those from the AON (Davis and Macrides, 1981). If this were the case, feedback from the piriform cortex will affect superficial cells less than feedback from AON. Because different types of information may be carried by superficial (tufted) and deeper (mitral) cells (Schneider and Scott, 1983; Orona et al., 1984; Scott et al., 1985; Nagayama et al., 2004, 2010), the distinct types of feedback may be optimized to affect different cell types. Inhibition routed through the glomerular layer is likely to affect all ''sister'' MCs similarly, but inhibition through GCs has the potential to have heterogeneous effects on ''sister'' MCs because of the differences in the spatial distribution of their lateral dendrites (Dhawale et al., 2010).

Our experiments also point to a difference in the glomerular projections of ipsilateral and contralateral axons from AON. Contralateral inputs are generally weaker, both anatomically and functionally. In addition, the reduced glomerular projection relative to the deeper layers may lead to differential effects on ''sister'' MCs for the same reasons discussed above. Contralateral inputs may also be spatially restricted, especially those that arise from AON pars externa (Reyher et al., 1988), leading to an impression of sparser innervation compared to the broader ipsilateral projections. AON neurons normally respond to ipsilateral nostril inputs, but latent inputs from the contralateral nostril could be unmasked if ipsilateral naris is obstructed (Kikuta et al., 2010), probably due to commissural projections of AON neurons (Brunjes et al., 2005; Hagiwara et al., 2012). The role the contralateral projections from the AON to the OB remains unclear, and future studies that target specific subregions of AON may be necessary, because different subregions of the AON may have distinct projection patterns (Reyher et al., 1988; Brunjes et al., 2005; Illig and Eudy, 2009).

Functional Consequences of AON Inputs for Bulbar Output

What are the consequences of activating AON inputs on MC activity? Our experiments in vitro indicate that the balance between excitation and inhibition favors an overall inhibitory effect, but excitation may be functional near threshold. When a MC is at rest, AON input does not induce firing, but when the cell is firing at low rates with the membrane potential close to threshold, AON input can trigger spikes that are precisely timed. Even though the excitation is rather mild, if a group of AON axons fire synchronously, they might activate precisely timed spikes in a sufficient number of MCs that might have a significant effect on their downstream targets. Intriguingly, when MCs are spiking robustly, AON inputs are mainly inhibitory. This is probably because at high rates of spiking, the fraction of time that the MC membrane potential is close to threshold (but not firing) is small.

Stimulating AON axons in vivo in the intact brain led to an increase in firing probability of MCs/TCs in a brief time window of a few milliseconds, as predicted by our in vitro studies. This remarkable effect was not anticipated by previous work, which has emphasized feedback innervation of GCs. Our slice experiments indicate that the excitation is particularly effective when MCs have moderate activity. It is intriguing that MCs are spontaneously active in vivo, particularly in awake animals (Rinberg et al., 2006). Feedback activation, therefore, could elicit precise synchronous spikes in a population of MCs, perhaps creating functional cell assemblies transiently. Synchronous activity in MCs, observed at different time scales (Kashiwadani et al., 1999; Doucette et al., 2011), could carry information that is readily decoded by downstream circuits (Luna and Schoppa, 2008; Davison and Ehlers, 2011). A recent study noted that synchronous spikes in MCs may be context dependent (Doucette et al., 2011); this could involve top-down modulation from the AON, providing brief excitation.

We did not find any evidence of rapid excitation triggered by AON activation during odor-evoked responses. There could be several reasons for this absence. First, even under the controlled conditions of slice experiments, we observed excitatory effects on spike activity in half the cells. Similarly, excitatory effects on spontaneous activity in vivo were also observed in only half the cells. It is possible that, by chance, all the cells in which odor-evoked responses were obtained fell in the nonresponsive half. A second, more likely, reason could be that the higher firing rates during odor responses masked any excitatory responses triggered by AON stimulation. Indeed, AON stimulation in slices caused much weaker excitatory effects on MCs at higher firing rates. Excitatory effects were observed in vivo when cells were firing spontaneously (6.9 ± 1.6 Hz), but not during odor responses, when the firing rates averaged 21.5 ± 4.0 Hz.

The excitatory effects in M/T cells caused by AON axon activity are followed by a strong inhibitory effect. This inhibition of spiking occurred soon after light stimulation, and lasted for a few hundred milliseconds. The time constant of recovery of firing was remarkably similar to the time constant of the slow component of inhibition recorded in vitro (189 versus 135 ms), suggesting that a brief synchronous activation of AON axons can suppress the output of the OB for a period that is governed by the time course of OB interneuron activity. AON neurons in vivo often respond in bursts of two to five spikes at 20–50 Hz locked to respiration, with maximal firing at the transition of inspiration-expiration (Lei et al., 2006; Kikuta et al., 2010).

Our findings also indicate that the effects of AON may be independent of the exact phase of respiration. If AON neurons are active during the time when MCs are active, they lead to a prompt reduction in firing rate. If AON axons are activated during a period when MCs are silent, fewer spikes are emitted by MCs in the ensuing period when their activity would have normally been high. The effects can be explained parsimoniously by simple algebraic summation of inhibition and excitation, although nonlinear effects could arise under other circumstances.

Together, the precisely timed excitation and long-lasting inhibition could play a role in suppressing background activity during specific periods of behavior, and also permit precisely timed spikes in MCs in a narrow time window. Our experiments suggest that excitatory odor responses are transiently suppressed (in terms of overall firing rates), but more complex temporal shaping of responses may occur because of interplay of intrinsic properties, sensory drive, and the feedback activity.

EXPERIMENTAL PROCEDURES

All procedures were performed using approved protocols in accordance with institutional (Harvard University Institutional Animal Care and Use Committee) and national guidelines.

Virus injections

Adeno-associated virus expressing ChR2-EYFP, purchased from Penn Vector Core (serotype9), was injected into Sprague-Dawley rat pups (postnatal days 5–7). Pups were anesthetized intraperitoneally with a ketamine (35 mg/kg) and xylazine (4 mg/kg) mixture and placed in a stereotactic apparatus. A small craniotomy was performed over the prefrontal cortex of the right hemisphere and viral solution was injected into the AON (stereotaxic coordinates: 1.6 mm lateral, 3.8 and 4.2 mm anterior from Bregma, and 4 mm deep from the brain surface; injection volume: 50 nl at two locations—total 100 nl—to span the full extent of AON) through a glass micropipette attached to a nanoinjector (MO-10, Narishige).

Slice Electrophysiology

Slice Preparation and Solutions

Two to four weeks postinjection, acute slices (300 μm) of the OB were obtained using standard procedures (Tyler et al., 2007). Briefly, horizontal sections were cut along the OB and the forebrain in ice-cold slicing solution containing 83 mM NaCl, 2.5 mM KCl, 3.3 mM $MgSO_4$, 1 mM NaH_2PO_4, 26.2 mM $NaHCO_3$, 22 mM glucose, 72 mM sucrose, and 0.5 mM $CaCl_2$, and equilibrated with 95% O_2/5% CO_2. Slices were transferred to a recording chamber and continuously perfused with normal artificial cerebrospinal fluid (ACSF) containing 119 mM NaCl, 2.5 mM KCl, 1.3 mM $MgSO_4$, 1 mM NaH_2PO_4, 26.2 mM $NaHCO_3$, 22 mM glucose, and 2.5 mM $CaCl_2$ equilibrated with 95% O_2/5% CO_2 at room temperature. Patch electrodes resistance was 3–5 MΩ for MCs and 5–7 MΩ for GCs and juxtaglomerular cells. For voltage-clamp recordings, we used Cs-gluconate based internal solution containing 130 mM D-gluconic acid, 130 mM CsOH, 5 mM NaCl, 10 mM HEPES, 12 mM phosphocreatine, 3 mM MgATP, 0.2 mM NaGTP, 1 mM EGTA, and 5 mg/ml biocytin. For current-clamp recordings, we used a K-gluconate based internal solution containing 130 mM KGlu, 10 mM HEPES, 10 mM phosphocreatine, 3 mM MgATP, 0.5 mM NaGTP, 0.2 mM EGTA, and 2.5 mM glutamate. Drugs were applied to slices through the perfusion system unless otherwise noted. In the case of selective block of GABAergic input within glomeruli, gabazine (SR-95531; 100 μM) was puff applied to the indicated location through a patch pipette (7–10 MΩ resistance) with pressure supplied by a Picospritzer (Parker Instrumentation) set to 500 ms puff duration and 10 psi.

Light Stimulation and Recordings

AMPA receptor-mediated EPSCs were recorded by holding cells at −70mV, whereas mixed AMPA and NMDA receptor-mediated EPSCs were recorded at +40mV. In select experiments, we added the $GABA_A$ receptor blockers picrotoxin (PTX, 0.1 mM, Tocris) or gabazine (SR-95531, 10 μM, Tocris) in the ACSF to prevent inhibitory responses. $GABA_A$ receptor-mediated IPSCs were recorded at 0mV, and for some cells both EPSCs and IPSCs were recorded at −40mV. ChR2 was activated in the entire optical field of view using a custom-built illuminator (Albeanu et al., 2008). A super-bright light-emitting diode (LED) array (CBT-120B, Luminus Devices) was coupled to the rear lamp-housing of an Olympus BX51 upright microscope, with an intensity of 5–10 mW/mm^2 in the sample plane. Stimulation sometimes elicited brief electric artifacts (from the LED power source) that were easily distinguished from synaptic currents and were not affected by blockers.

Juxtaglomerular Cell Type Identification

We relied on published characterization of juxtaglomerular cells to identify ETCs, PGCs, and SACs (Hayar et al., 2004; Gire and Schoppa, 2009; Shao et al., 2009). ETCs were identified in a few recordings based on their bursts of spikes in cell-attached recordings. They were mainly identified based on their location in the border between glomeruli and EPL, their lower input resistance (194 ± 32 MΩ in Hayar et al., 2004) and the absence of spontaneous bursts of synaptic input (Figure S3; compare Figure 1 of Hayar et al., 2004). Conversely, SACs and PGCs almost always have bursting spontaneous synaptic activity (Hayar et al., 2004). In addition, PGCs have much higher input resistance (1,054 ± 106 MΩ, in Hayar et al., 2004). There remains some uncertainty about lower input resistance SACs, but these will comprise a small fraction of our total sample.

Data Acquisition and Analysis

Responses were recorded with an Axopatch 200B amplifier (Molecular Devices), filtered at 2 kHz, and digitized at 20 kHz (Axon Digi1440A) using PClamp acquisition software (Molecular Devices). The recorded data were analyzed using Clampfit (Version 10.1.0.10, Molecular Devises). We used the peak amplitudes of synaptic currents recorded at −70mV to characterize AMPA EPSCs, and the amplitude at 50 ms to estimate the contribution of NMDA to EPSCs (AMPA currents are negligible at this time point) from the currents recorded at +40mV. Latencies were measured as time between light onset and the onset of synaptic currents, detected as a systematic deviation of more than 3 SDs from baseline noise. The effects of light stimulation on the firing rates of MCs were analyzed in the same manner as that described below in section on PSTH significance analysis for the in vivo data. Summary data are reported as mean ± SD, and all statistical tests were Student's t test unless noted otherwise.

Post Hoc Anatomy

After recordings, slices were fixed overnight in 4% paraformaldehyde solution in PBS, at 4°C. To confirm the injection site, samples were imaged with a confocal or a tiling wide-field imaging microscope (LSM 510 or Axio Imager Z2, Zeiss). To identify the recorded cells, biocytin was reacted to streptavidin conjugated with Alexa 594 (Invitrogen) in 0.1% PBS-Tx overnight and samples were imaged with a Zeiss LSM 510 and 710 confocal microscope. The fluorescence intensity of confocal images was analyzed by image processing in ImageJ.

In Vivo Electrophysiology

Surgery

Two to five weeks postinjection rats were anesthetized with ketamine (100 mg/kg)/xylazine (10 mg/kg). A head-fixing plate was glued on the skull a small craniotomy was performed over the right bulb, ipsilateral to the injected AON, and the dura was removed.

Light Stimulation and Recordings

Extracellular signals from MCs were recorded with sharp tungsten electrodes (1–10 MΩ; FHC). Breathing signals were monitored with a piezoelectric stress sensor (Kent Scientific) that was wrapped around the mouse thorax. MCs were identified based on depth, respiration related firing pattern, and by monitoring the activity levels in more superficial layers. ChR2 was activated with a blue laser (450 nm, ~60 mW/mm^2 on the brain surface). Stimuli consisted of a pair of 40 ms pulses of light delivered 50 ms apart. Light intensity for in vivo experiments was greater than that used for in vitro experiments to ensure adequate penetration of the light through tissue. In both sets of experiments, light intensity and duration was kept within limits that typically do not cause heating effects in tissue (Cardin et al., 2010; Han, 2012).

Odor Delivery

Odors were delivered from a custom-built olfactometer containing the following odors: methyl tiglate, ethyl valerate, isopropyl tiglate, ethyl butyrate, hexanal, heptanal, and isoamyl acetate. All odors were dissolved in diethylphthalate to a concentration of 10%. Odors were delivered by a stream of clean air (0.6 l/m) that was passed through vials containing the diluted odors. The airflow at the nose port was constant to ensure that that the responses obtained are not caused by a sudden change in air flow near the nose. Odors were delivered for 5 s every 45 s.

Data Acquisition and Analysis

Signals were amplified and filtered: 300 Hz to 5 kHz (A-M systems). Both breathing and MC activity signals were acquired at 20 kHz sampling and digitized with 16 bit precision (National Instruments). Data were analyzed using MATLAB (MathWorks). Spikes were sorted manually based on their projections in the principal component space and a refractory period was used for validation. Only single unit data are presented here. For analysis of the breathing signals, we defined peak inhalation as phase zero. Summary data are reported as mean ± SD, and all statistical tests were Student's t test unless noted otherwise

PSTH Significance Analysis

Excitatory responses in the in vivo data were measured by generating PSTHs with 1 ms bins and finding the highest firing within the first 10 ms following light stimulation. To measure the significance of these responses, we used the following bootstrapping method. First, 100,000 control PSTHs were generated where firing was aligned to random times instead of the light stimulus. We then compared the excitatory response to the distribution of firing rates at the same bin of all randomly aligned PSTHs. Excitatory responses were considered significant if less than 0.001 of the random PSTHs had values above the real response.

Post Hoc Anatomy

To confirm the injection site, animals used for recordings were perfused transcardially with 20 ml PBS first, followed by 50 ml of 4% paraformaldehyde and 10% picric acid in 0.1 M phosphate buffer (pH 7.4). Brains were removed, postfixed in 4% paraformaldehyde overnight at 4°C, cut into 100-μm-thick sagittal sections, and imaged with epifluorescence microscope (Axio Imager Z2, Zeiss).

SUPPLEMENTAL INFORMATION

Supplemental Information includes five figures and can be found with this article online at http://dx.doi.org/10.1016/j.neuron.2012.10.028.

ACKNOWLEDGMENTS

F.M. was supported by a Swiss National Foundation Fellowship and D.R. was supported by the Edmond and Lily Safra Center for Brain Sciences, Hebrew University. Work in V.N.M.'s laboratory related to this project was supported by Harvard University and by the NIH. We thank the Harvard Center for Biological Imaging and Professor Catherine Dulac for the use of microscopes to image fixed tissue.

Accepted: October 19, 2012
Published: December 19, 2012

REFERENCES

Albeanu, D.F., Soucy, E., Sato, T.F., Meister, M., and Murthy, V.N. (2008). LED arrays as cost effective and efficient light sources for widefield microscopy. PLoS ONE *3*, e2146.

Balu, R., and Strowbridge, B.W. (2007). Opposing inward and outward conductances regulate rebound discharges in olfactory mitral cells. J. Neurophysiol. *97*, 1959–1968.

Balu, R., Pressler, R.T., and Strowbridge, B.W. (2007). Multiple modes of synaptic excitation of olfactory bulb granule cells. J. Neurosci. *27*, 5621–5632.

Baluch, F., and Itti, L. (2011). Mechanisms of top-down attention. Trends Neurosci. *34*, 210–224.

Bardy, C., Alonso, M., Bouthour, W., and Lledo, P.M. (2010). How, when, and where new inhibitory neurons release neurotransmitters in the adult olfactory bulb. J. Neurosci. *30*, 17023–17034.

Boyd, A.M., Sturgill, J.F., Poo, C., and Isaacson, J.S. (2012). Cortical feedback control of olfactory bulb circuits. Neuron *76*, this issue, 1161–1174.

Brunjes, P.C., Illig, K.R., and Meyer, E.A. (2005). A field guide to the anterior olfactory nucleus (cortex). Brain Res. Rev. *50*, 305–335.

Cardin, J.A., Carlén, M., Meletis, K., Knoblich, U., Zhang, F., Deisseroth, K., Tsai, L.-H., and Moore, C.I. (2010). Targeted optogenetic stimulation and recording of neurons in vivo using cell-type-specific expression of Channelrhodopsin-2. Nat. Protoc. *5*, 247–254.

Carlson, G.C., Shipley, M.T., and Keller, A. (2000). Long-lasting depolarizations in mitral cells of the rat olfactory bulb. J. Neurosci. *20*, 2011–2021.

Christie, J.M., and Westbrook, G.L. (2006). Lateral excitation within the olfactory bulb. J. Neurosci. *26*, 2269–2277.

Cury, K.M., and Uchida, N. (2010). Robust odor coding via inhalation-coupled transient activity in the mammalian olfactory bulb. Neuron *68*, 570–585.

Davis, B.J., and Macrides, F. (1981). The organization of centrifugal projections from the anterior olfactory nucleus, ventral hippocampal rudiment, and piriform cortex to the main olfactory bulb in the hamster: an autoradiographic study. J. Comp. Neurol. *203*, 475–493.

Davis, B.J., Macrides, F., Youngs, W.M., Schneider, S.P., and Rosene, D.L. (1978). Efferents and centrifugal afferents of the main and accessory olfactory bulbs in the hamster. Brain Res. Bull. *3*, 59–72.

Davison, I.G., and Ehlers, M.D. (2011). Neural circuit mechanisms for pattern detection and feature combination in olfactory cortex. Neuron *70*, 82–94.

de Olmos, J., Hardy, H., and Heimer, L. (1978). The afferent connections of the main and the accessory olfactory bulb formations in the rat: an experimental HRP-study. J. Comp. Neurol. *181*, 213–244.

De Saint Jan, D., Hirnet, D., Westbrook, G.L., and Charpak, S. (2009). External tufted cells drive the output of olfactory bulb glomeruli. J. Neurosci. *29*, 2043–2052.

Deisseroth, K. (2011). Optogenetics. Nat. Methods *8*, 26–29.

Dhawale, A.K., Hagiwara, A., Bhalla, U.S., Murthy, V.N., and Albeanu, D.F. (2010). Non-redundant odor coding by sister mitral cells revealed by light addressable glomeruli in the mouse. Nat. Neurosci. *13*, 1404–1412.

Doucette, W., Gire, D.H., Whitesell, J., Carmean, V., Lucero, M.T., and Restrepo, D. (2011). Associative cortex features in the first olfactory brain relay station. Neuron *69*, 1176–1187.

Egger, V., and Urban, N.N. (2006). Dynamic connectivity in the mitral cell-granule cell microcircuit. Semin. Cell Dev. Biol. *17*, 424–432.

Fontanini, A., and Katz, D.B. (2009). Behavioral modulation of gustatory cortical activity. Ann. N Y Acad. Sci. *1170*, 403–406.

Gire, D.H., and Schoppa, N.E. (2009). Control of on/off glomerular signaling by a local GABAergic microcircuit in the olfactory bulb. J. Neurosci. *29*, 13454–13464.

Gire, D.H., Franks, K.M., Zak, J.D., Tanaka, K.F., Whitesell, J.D., Mulligan, A.A., Hen, R., and Schoppa, N.E. (2012). Mitral cells in the olfactory bulb are mainly excited through a multistep signaling path. J. Neurosci. *32*, 2964–2975.

Hagiwara, A., Pal, S.K., Sato, T.F., Wienisch, M., and Murthy, V.N. (2012). Optophysiological analysis of associational circuits in the olfactory cortex. Front Neural Circuits *6*, 18.

Han, X. (2012). Optogenetics in the nonhuman primate. Prog. Brain Res. *196*, 215–233.

Hayar, A., Karnup, S., Ennis, M., and Shipley, M.T. (2004). External tufted cells: a major excitatory element that coordinates glomerular activity. J. Neurosci. *24*, 6676–6685.

Hurley, L.M., Devilbiss, D.M., and Waterhouse, B.D. (2004). A matter of focus: monoaminergic modulation of stimulus coding in mammalian sensory networks. Curr. Opin. Neurobiol. *14*, 488–495.

Illig, K.R., and Eudy, J.D. (2009). Contralateral projections of the rat anterior olfactory nucleus. J. Comp. Neurol. *512*, 115–123.

Isaacson, J.S. (2010). Odor representations in mammalian cortical circuits. Curr. Opin. Neurobiol. *20*, 328–331.

Isaacson, J.S., and Strowbridge, B.W. (1998). Olfactory reciprocal synapses: dendritic signaling in the CNS. Neuron *20*, 749–761.

Isaacson, J.S., and Scanziani, M. (2011). How inhibition shapes cortical activity. Neuron *72*, 231–243.

Kapoor, V., and Urban, N.N. (2006). Glomerulus-specific, long-latency activity in the olfactory bulb granule cell network. J. Neurosci. *26*, 11709–11719.

Kashiwadani, H., Sasaki, Y.F., Uchida, N., and Mori, K. (1999). Synchronized oscillatory discharges of mitral/tufted cells with different molecular receptive ranges in the rabbit olfactory bulb. J. Neurophysiol. *82*, 1786–1792.

Kay, L.M., and Laurent, G. (1999). Odor- and context-dependent modulation of mitral cell activity in behaving rats. Nat. Neurosci. *2*, 1003–1009.

Kikuta, S., Kashiwadani, H., and Mori, K. (2008). Compensatory rapid switching of binasal inputs in the olfactory cortex. J. Neurosci. *28*, 11989–11997.

Kikuta, S., Sato, K., Kashiwadani, H., Tsunoda, K., Yamasoba, T., and Mori, K. (2010). From the Cover: Neurons in the anterior olfactory nucleus pars externa detect right or left localization of odor sources. Proc. Natl. Acad. Sci. USA *107*, 12363–12368.

Kiselycznyk, C.L., Zhang, S., and Linster, C. (2006). Role of centrifugal projections to the olfactory bulb in olfactory processing. Learn. Mem. *13*, 575–579.

Knudsen, E.I. (2007). Fundamental components of attention. Annu. Rev. Neurosci. *30*, 57–78.

Lei, H., Mooney, R., and Katz, L.C. (2006). Synaptic integration of olfactory information in mouse anterior olfactory nucleus. J. Neurosci. *26*, 12023–12032.

Luna, V.M., and Schoppa, N.E. (2008). GABAergic circuits control input-spike coupling in the piriform cortex. J. Neurosci. *28*, 8851–8859.

Macrides, F., and Chorover, S.L. (1972). Olfactory bulb units: activity correlated with inhalation cycles and odor quality. Science *175*, 84–87.

Matsutani, S., and Yamamoto, N. (2008). Centrifugal innervation of the mammalian olfactory bulb. Anat. Sci. Int. *83*, 218–227.

Miesenböck, G. (2009). The optogenetic catechism. Science *326*, 395–399.

Nagayama, S., Takahashi, Y.K., Yoshihara, Y., and Mori, K. (2004). Mitral and tufted cells differ in the decoding manner of odor maps in the rat olfactory bulb. J. Neurophysiol. *91*, 2532–2540.

Nagayama, S., Enerva, A., Fletcher, M.L., Masurkar, A.V., Igarashi, K.M., Mori, K., and Chen, W.R. (2010). Differential axonal projection of mitral and tufted cells in the mouse main olfactory system. Front Neural Circuits *4*.

Najac, M., De Saint Jan, D., Reguero, L., Grandes, P., and Charpak, S. (2011). Monosynaptic and polysynaptic feed-forward inputs to mitral cells from olfactory sensory neurons. J. Neurosci. *31*, 8722–8729.

Nicoll, R.A., and Jahr, C.E. (1982). Self-excitation of olfactory bulb neurones. Nature *296*, 441–444.

Nissant, A., Bardy, C., Katagiri, H., Murray, K., and Lledo, P.M. (2009). Adult neurogenesis promotes synaptic plasticity in the olfactory bulb. Nat. Neurosci. *12*, 728–730.

Noudoost, B., Chang, M.H., Steinmetz, N.A., and Moore, T. (2010). Top-down control of visual attention. Curr. Opin. Neurobiol. *20*, 183–190.

Orona, E., Rainer, E.C., and Scott, J.W. (1984). Dendritic and axonal organization of mitral and tufted cells in the rat olfactory bulb. J. Comp. Neurol. *226*, 346–356.

Petreanu, L., Huber, D., Sobczyk, A., and Svoboda, K. (2007). Channelrhodopsin-2-assisted circuit mapping of long-range callosal projections. Nat. Neurosci. *10*, 663–668.

Petzold, G.C., Hagiwara, A., and Murthy, V.N. (2009). Serotonergic modulation of odor input to the mammalian olfactory bulb. Nat. Neurosci. *12*, 784–791.

Pimentel, D.O., and Margrie, T.W. (2008). Glutamatergic transmission and plasticity between olfactory bulb mitral cells. J. Physiol. *586*, 2107–2119.

Pinching, A.J., and Powell, T.P. (1972). The termination of centrifugal fibres in the glomerular layer of the olfactory bulb. J. Cell Sci. *10*, 621–635.

Pírez, N., and Wachowiak, M. (2008). In vivo modulation of sensory input to the olfactory bulb by tonic and activity-dependent presynaptic inhibition of receptor neurons. J. Neurosci. *28*, 6360–6371.

Pouille, F., and Scanziani, M. (2001). Enforcement of temporal fidelity in pyramidal cells by somatic feed-forward inhibition. Science *293*, 1159–1163.

Powell, T.P., Cowan, W.M., and Raisman, G. (1965). The central olfactory connexions. J. Anat. *99*, 791–813.

Price, J.L., and Powell, T.P. (1970). An experimental study of the origin and the course of the centrifugal fibres to the olfactory bulb in the rat. J. Anat. *107*, 215–237.

Rennaker, R.L., Chen, C.F., Ruyle, A.M., Sloan, A.M., and Wilson, D.A. (2007). Spatial and temporal distribution of odorant-evoked activity in the piriform cortex. J. Neurosci. *27*, 1534–1542.

Restrepo, D., Doucette, W., Whitesell, J.D., McTavish, T.S., and Salcedo, E. (2009). From the top down: flexible reading of a fragmented odor map. Trends Neurosci. *32*, 525–531.

Reyher, C.K., Schwerdtfeger, W.K., and Baumgarten, H.G. (1988). Interbulbar axonal collateralization and morphology of anterior olfactory nucleus neurons in the rat. Brain Res. Bull. *20*, 549–566.

Rinberg, D., Koulakov, A., and Gelperin, A. (2006). Sparse odor coding in awake behaving mice. J. Neurosci. *26*, 8857–8865.

Schneider, S.P., and Scott, J.W. (1983). Orthodromic response properties of rat olfactory bulb mitral and tufted cells correlate with their projection patterns. J. Neurophysiol. *50*, 358–378.

Schoppa, N.E., Kinzie, J.M., Sahara, Y., Segerson, T.P., and Westbrook, G.L. (1998). Dendrodendritic inhibition in the olfactory bulb is driven by NMDA receptors. J. Neurosci. *18*, 6790–6802.

Scott, J.W., Ranier, E.C., Pemberton, J.L., Orona, E., and Mouradian, L.E. (1985). Pattern of rat olfactory bulb mitral and tufted cell connections to the anterior olfactory nucleus pars externa. J. Comp. Neurol. *242*, 415–424.

Shao, Z., Puche, A.C., Kiyokage, E., Szabo, G., and Shipley, M.T. (2009). Two GABAergic intraglomerular circuits differentially regulate tonic and phasic presynaptic inhibition of olfactory nerve terminals. J. Neurophysiol. *101*, 1988–2001.

Shao, Z., Puche, A.C., Liu, S., and Shipley, M.T. (2012). Intraglomerular inhibition shapes the strength and temporal structure of glomerular output. J. Neurophysiol. *108*, 782–793.

Shepherd, G.M., Chen, W.R., and Greer, C.A. (2004). Olfactory bulb. In The Synaptic Organization of the Brain, G.M. Shepherd, ed. (New York: Oxford University Press), pp. 165–216.

Shipley, M.T., and Adamek, G.D. (1984). The connections of the mouse olfactory bulb: a study using orthograde and retrograde transport of wheat germ agglutinin conjugated to horseradish peroxidase. Brain Res. Bull. *12*, 669–688.

Shusterman, R., Smear, M.C., Koulakov, A.A., and Rinberg, D. (2011). Precise olfactory responses tile the sniff cycle. Nat. Neurosci. *14*, 1039–1044.

Stettler, D.D., and Axel, R. (2009). Representations of odor in the piriform cortex. Neuron *63*, 854–864.

Strowbridge, B.W. (2009). Role of cortical feedback in regulating inhibitory microcircuits. Ann. N Y Acad. Sci. *1170*, 270–274.

Tyler, W.J., Petzold, G.C., Pal, S.K., and Murthy, V.N. (2007). Experience-dependent modification of primary sensory synapses in the mammalian olfactory bulb. J. Neurosci. *27*, 9427–9438.